

---

# Near Real-Time Social Distancing in London

---

James Walsh<sup>1</sup>, Oluwafunmilola Kesa<sup>2</sup>, Andrew Wang<sup>4</sup>, Mihai Ilas<sup>4</sup>, Patrick O’Hara<sup>2</sup>, Oscar Giles<sup>1</sup>, Neil Dhir<sup>1,2</sup>, Theodoros Damoulas<sup>1,2,3</sup>

<sup>1</sup>The Alan Turing Institute  
{jwalsh, ogiles, ndhir}@turing.ac.uk

Departments of <sup>2</sup>Computer Science and <sup>3</sup>Statistics, University of Warwick  
{funmi.kesa, patrick.h.o-hara, t.damoulas}@warwick.ac.uk

<sup>4</sup>Engineering Department, University of Cambridge  
{aslw3, mai32}@cam.ac.uk

## Abstract

During the COVID-19 pandemic, policy makers at the Greater London Authority, the regional governance body of London, UK, are reliant upon prompt and accurate data sources. Large well-defined heterogeneous compositions of activity throughout the city are sometimes difficult to acquire, yet are a necessity in order to learn ‘busyness’ and consequently make safe policy decisions. One component of our project within this space is to utilise existing infrastructure to estimate social distancing adherence by the general public. Our method enables near immediate sampling and contextualisation of activity and physical distancing on the streets of London via live traffic camera feeds. We introduce a framework for inspecting and improving upon existing methods, whilst also describing its active deployment on over 900 real-time feeds.

## Introduction

Sources of public data regarding the current global pandemic fail to meet a number of requirements: accuracy in recorded measure, spatial and temporal granularity, and most importantly accessibility to policy makers and the general public. As the global community is actively engaged in understanding more about the effects and transmission mechanism of COVID-19, many governments are enacting temporary restrictions targeted at reducing the proximity of the public to one another (i.e. ‘social distancing’). These have become known as “lock-downs” [16], and the monitoring of public response to these measures have come out of necessity for policy makers to better understand their adoption, plan economic recovery and eventual suspension. When social restrictions were first implemented in the UK there were limited options to measure *activity*. A number of private companies trading in public movement data began providing aggregate information at the request of local government, from sources such as workplace reporting, wearable sports activity trackers and point of sale transactions. It became clear there was an immediate need for additional response metrics for activity, unmet in the aforementioned sources. Here, we describe a *social-distancing estimation system* using Open Government Licensed [9] traffic cameras directed towards pedestrian crossings and pavements, reporting to policy makers in near real-time. This work includes the description of our pipeline and new accuracy results on urban footage benchmarks. Due to the nature of this work, there are substantial privacy concerns, all footage employed is anonymised through restrictive sampling and systematically undergoes continuous review by our organisation’s Ethical Advisory Panel.

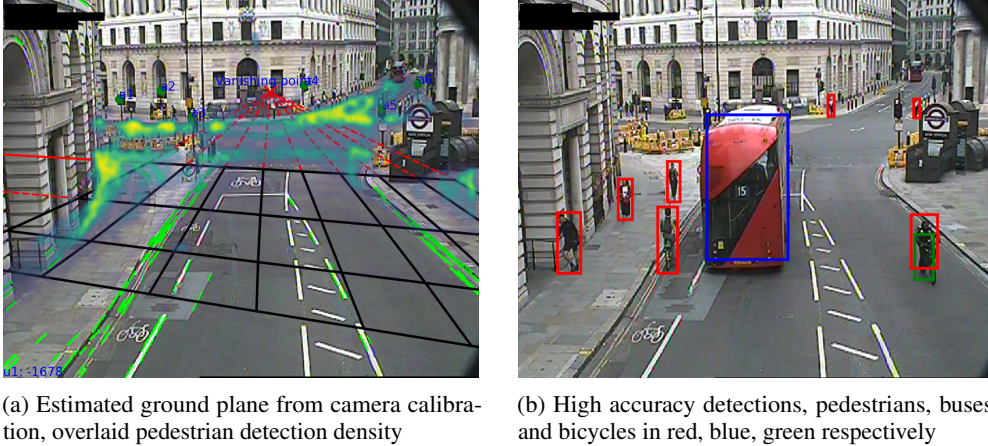


Figure 1: Example of our method applied to a traffic camera at Bank, London

## Method

Our method starts with the calibration of each camera we expect to receive samples from, this Camera Calibration is a one-time process to learn parameters for mapping from the 2D scene to a 3D real-world representation. Once complete, active data collection occurs continuously to ingest samples from the public domain, upon successful retrieval each clip is queued for object detection by the inference cluster. Upon exiting the detection stage, each pedestrian detection is transformed to the learned world-plane representation. These results are submitted to the database, upon which other digital twin components will be simultaneously retrieving and processing to watch for spikes or irregularities in selected areas of concern.

**1 Camera Calibration** Obtaining a world-plane mapping of a camera scene is extensively described in the computer vision literature. A large portion of literature requires manual calibration using known patterns to estimate the transformation [2, 7, 23]. Vanishing line estimation is essential for perspective transformation [4]. [18, 6] use the activity of a large number of vehicles travelling parallel and regularly to find the vanishing point. [10, 22, 5, 8] calibrate the camera using clear, regular or known lines in the scene, which is not practical for the case of a large spread of different cameras. The stratified transformation discussed in [11] relies on the fact that there are many lines to be extracted from high quality images to build a real-world model. [18], [22], [5] and [3] extract visible road features by using a derivative-based binarisation operator. This is only suitable for cameras overlooking straight and visually similar lanes. Overall, our method is more easily generalised to higher quantity of cameras with cluttered urban traffic scenes and lower resolution.

The mapping,  $(u, v, 0) \mapsto (X, Y, Z)$ , from the image plane to world geometry is sought, where there is no *a priori* truth of the camera parameters. The *intrinsics* (focal length, principal point, skew and aspect ratio) and *extrinsics* (positioning and direction) therefore must be estimated or assumed. The cameras have the following limitations: Roads have non-zero curvature or have junctions and vary in width; Irregular road markings of varying quality; Cameras have low resolution, changing lighting in very short sample duration. To maintain robustness we make the following internal camera assumptions: **(a)** unit aspect ratio and constant skew; **(b)** coincidence of principal point and image centre; these are commonplace and rarely estimated due to lack of visual information [4], [6]. External assumptions are as following; **(c)** zero radial distortion; **(d)** flat horizon  $v_0 = v_1$ ; **(e)** zero-incline road  $Z = 0$ ; these seem reasonable by manual inspection of 100 random cameras and must be made given the above limitations. If cameras where these assumptions do not hold, a pre-processing stage using additional information can be implemented to correct radial distortion [6], inclined horizon (setting  $v_1 \neq v_0$ ), and non-zero inclination  $Z$  [19].

This simplified pinhole camera model allows the transformation to be described by four parameters  $u_0, v_0, u_1, h$  where  $(u_0, v_0), (u_1, v_0)$  are the vanishing points of two orthogonal planar directions subtending the horizon line, and  $h$  is the height of the camera above ground (Figure B.1). Parallel lines on the road and on cars, such as road edges, advanced stop lines and car and truck edges, are used to estimate this transformation (Figure 2).

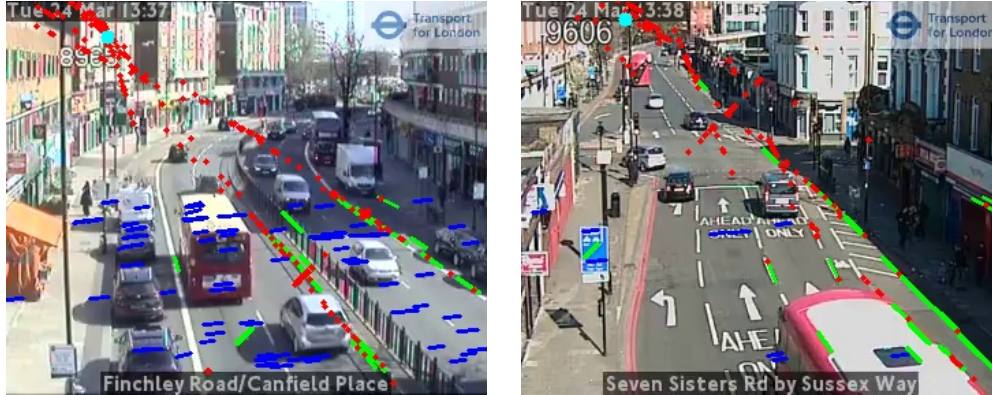


Figure 2: Lines detected by our feature extraction algorithm, two orthogonal sets of lines: those parallel to the foreground road (green, *road edges*) and those perpendicular (blue, *road perpendiculars*). The intersection of each set, the vanishing point (light blue) which lies on the horizon. The challenging conditions are shown here, including varying lighting and non-zero road curvature.

The Canny edge detector [21] is applied per frame to find sets of *road edges* and *road perpendiculars* as shown in Figure 2. The Hough transform matches collinear edge segments into linked lines which are then filtered by gradient [18] and dimensions. The vanishing point is then simply the maximum histogram density estimate of the pairwise line intersections. This is chosen over more expensive MLE methods [24] where the vanishing point error is optimised using least squares [4], [3] or Levenberg–Marquardt [18], [11]. This procedure is repeated across different contrast factors to provide a robust line detector in challenging lighting conditions. Finally,  $u_0, u_1, v_0$  values are averaged over all frames to extract maximum information when the videos are sparsely populated with vehicles. Finally, the camera height  $h$  can be manually calculated by transforming an object of known dimensions. For example, using frequently appearing London buses of fixed 2.52m width, the calculated height averages  $h = 9.6m$  with 10% average deviation across 7 randomly picked cameras. Other ways to obtain the scale  $h$  include using car length averages [19] or known lane spacings [8, 3].

**2 Data Collection** Transport for London (TFL) sourced footage selected for this platform consists of ten-second videos from 911 live cameras every four-minutes from the Open Roads initiative, known as JamCams [15]. A day of collection constitutes 220,000 individual files of a total of 20-30GB, deleted upon processing in accordance with our data retention policy. The nature of monitoring public spaces means we cannot *a priori* request consent. We limit the resolution of our collected footage to inhibit any capacity to personally identify an individual. Thus only their humanoid likeness is utilised for detection.

**3 Object Detection** In order to detect entities quickly enough to assist policy makers, we evaluated object detection models such as SSD [13], YOLO v3 [17] & YOLO v4 [1] to balance speed with accuracy. These are typically determined by architecture, model depth, input sizes, classification cardinality and execution environment. You Only Look Once (YOLO) is a one-stage anchor-based object detector that is both fast and accurate. YOLOv3 achieves an accuracy of 57.9  $AP_{50}$  in 51ms [17]. Recently, a faster version named YOLOv4, was released with a state-of-the-art accuracy than alternative object detectors. Notably, YOLOv4 can be trained and used on conventional GPUs which allows for faster experimentation and fine-tuning on custom datasets. YOLOv4 improves performance and speed by 10% and 12% respectively [1]. We employ both YOLOv3 & v4 in our experiments. Each were pretrained on Coco [12] dataset, a large-scale repository of objects belonging to 80 class labels. Due to our objective, the classes of interest are limited to six labels: person, car, bus, motorbike, bicycle, and truck. We fine-tuned the model on six labels using joint datasets from COCO and MIO-TCD [14], and then evaluated them against. Results in the evaluation section shows that fine-tuning the traffic camera footage.

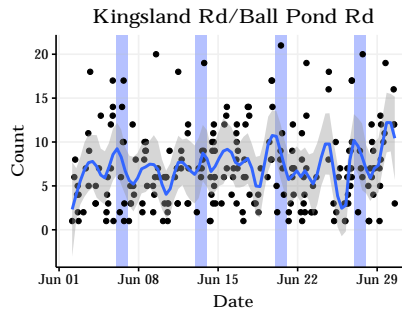


Figure 3: Pedestrians in samples from Kingsland Rd/Ball Pond Rd, June 2020

	Datasets	person	bicycle	car	motorbike	bus	truck
<i>Train</i>	Coco 2017	262 465	7113	43 867	8725	6069	9973
	MIO-TCD	5760	1758	186 767	1484	8443	54 340
<i>Validation</i>	Coco 2017	11 004	316	1932	371	285	415
	MIO-TCD	1368	502	46 730	353	2155	13 694
	Jamcam	1233	106	7867	106	203	1982

Table 1: Training and Validation Dataset Statistics

**4 Social distancing** To measure distance within this scene we may find the Euclidean distance between pedestrian detections after the above *world plane* projection. We elected to improve in areas of high pedestrian use by employing points of reference via *geotagged* static urban furniture, such as traffic lights.

We first select an appropriate flat 2D projected coordinate reference system, British National Grid (OS 27700). Then, we create a second transformation between these two 2D Cartesian frames of

$$\begin{bmatrix} x' + e_x \\ y' + e_y \\ 0 \end{bmatrix} = \begin{bmatrix} k_1 \cos(\theta) & k_3 \sin(\theta) & t_x \\ -k_2 \sin(\theta) & k_4 \cos(\theta) & t_y \\ 0 & 0 & 1 \end{bmatrix} \begin{bmatrix} x \\ y \\ 0 \end{bmatrix}$$

reference, represented below with scale and shear factors,  $k$ , angle of rotation,  $\theta$ , translations  $t$ , and error terms,  $e$ . The estimated *real world plane* is then generated from the optimisation of the sum of squares error.

## Evaluation

**Camera calibration** Uncertainty in the estimation of the vanishing line and extrinsic camera height arises due to imperfect camera effects eliminated in the assumptions and inaccurate automatic line extraction. The estimated errors in mapped world position  $dX, dY$ , are evaluated for 3 randomly selected cameras which are manually calibrated beforehand using the total differential over all estimated parameters  $p_i \in \{u_0, v_0, u_1, h\}$  assuming that the vehicle tracking  $u, v$  are accurate at the point of evaluation. The average relative uncertainty in position mapping due to parameter estimation  $|\frac{dX}{X}|$  is calculated to be 17.7%,  $\sigma = 7.9\%$ .

**Object detection** As preprocessing steps, we subset 6 labels from the Coco 2017 and MIO-TCD localization dataset. Unlike the Coco dataset, MIO-TCD localization dataset contains 11 labels with additional categories such as motorized vehicle, non-motorized vehicle, pickup truck, single unit truck, and work van, not found in the Coco 2017 dataset. For comparison, we collapse the different categories of trucks as *truck* and remove labels regarding vehicle motorization. We produced new collection of manually labelled entities specifically on frames from traffic cameras, using CVAT [20]. The dataset contains 1142 frames and 11497 bounding boxes as shown in Table 1. For evaluation/validation, we compute the mean Average Precision (mAP) at IOU threshold of 0.5 over the Coco 2017, MIO-TCD, joint (Coco 2017 + MIO-TCD), and *JamCam* datasets.

We fine-tune a pretrained YOLOv4 weights file on six labels from different training datasets using a batch size of 16, subdivisions of 4, image size of 416 and at least 7000 iterations on a Tesla V100-SXM3-32GB GPU. We train three different models on 1) Coco 2017 training data 2) MIO-TCD training data 3) Joint data containing random shuffle of Coco 2017 and MIO-TCD training data. Table 1 shows the number of training data by labels. The validation data contains Coco 2017 validation data, MIO-TCD validation data and Jamcam data.

The performances of the three models are shown in Table 2. On the Coco 2017 validation data, the model achieves a mean Average Precision (mAP@0.50) of 67.55 %. However, the model trained on Coco 2017 dataset performed poorly on MIO-TCD localization validation dataset with an mAP of 20.39 %. Likewise, the performance of the model trained on MIO-TCD dataset reduces greatly from 85.80 % to 14.24 % when Coco 2017 dataset is used as the validation dataset. This behaviour

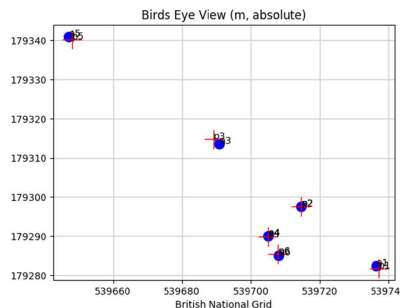


Figure 4: Estimated locations of urban furniture (green) and pedestrians (blue) on British National Grid



Training	Validation	mAP@0.50 $\uparrow$	Precision $\uparrow$	Recall $\uparrow$	F1-score $\uparrow$
Coco	Coco	<b>67.55</b>	<b>0.73</b>	<b>0.70</b>	<b>0.71</b>
	MIO-TCD	20.39	0.38	0.49	0.43
	JamCam	41.64	0.62	0.59	0.60
MIO-TCD	Coco	14.24	0.35	0.30	0.30
	MIO-TCD	<b>85.80</b>	<b>0.83</b>	<b>0.90</b>	<b>0.86</b>
	JamCam	35.12	0.75	0.45	0.57
Joint	Coco	64.56	0.71	0.69	0.70
	MIO-TCD	<b>80.32</b>	<b>0.79</b>	<b>0.88</b>	<b>0.83</b>
	JamCam	46.53	0.76	0.57	0.65

Table 2: Comparing models fine-tuned on the Coco 2017 dataset, MIO-TCD dataset, and joint training set using YOLOv4 architecture.

might be as a result of the differences in the resolutions and weather conditions in the two datasets. Performing a joint training creates a balance between the two datasets and increases the model’s performance on the independent Jamcam dataset.

## Conclusion

This work contributes improved accuracy upon the state of the art detection model for the urban domain, introduces a camera perspective estimation method, and demonstrates how multiple machine learning techniques may directly benefit public health. Combined with large-scale, inexpensive consumer distributed computing infrastructure, Figure A.1, we provide an option for policy makers to receive an almost real-time perspective of their impact via an online interface, Figure A.2. Ongoing directions for our project include validating our early warning detection system, improving the Digital Twin’s overall accuracy in providing "human-in-the-loop" recommendations for policy makers, and continuing to increase the transparency and ease of use for our stakeholders and the general public.

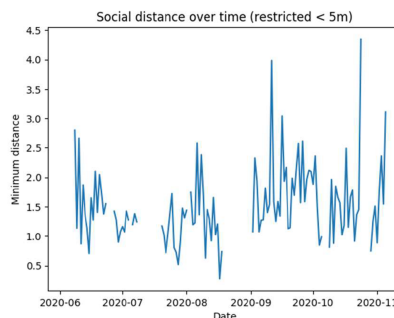


Figure 5: Pedestrians in samples from Kingsland Rd/Ball Pond Rd, June 2020

## Acknowledgements and Disclosure of Funding

Funded by Lloyd’s Register Foundation programme on Data Centric Engineering and Warwick Impact Fund via the EPSRC Impact Acceleration Account. Further supported by the Greater London Authority, Transport for London, Microsoft, Department of Engineering at University of Cambridge and the Science and Technology Facilities Council. We would like to thank Sam Blakeman and James Brandreth for their help on multiple aspects of this work.

## References

- [1] Bochkovskiy, A., Wang, C.-Y., and Liao, H.-Y. M. Yolov4: Optimal speed and accuracy of object detection, 2020.
- [2] Caprile, B. and Torre, V. Using vanishing points for camera calibration. *International Journal of Computer Vision*, 4(2):127–139, March 1990. ISSN 1573-1405. doi: 10.1007/BF00127813. URL <https://doi.org/10.1007/BF00127813>.
- [3] Cathey, F. and Dailey, D. A novel technique to dynamically measure vehicle speed using uncalibrated roadway cameras. In *IEEE Proceedings. Intelligent Vehicles Symposium, 2005.*, pp. 777–782. IEEE, 2005.
- [4] Criminisi, A. *Accurate Visual Metrology from Single and Multiple Uncalibrated Images*. Springer London, London, 2001. ISBN 978-1-4471-1040-8 978-0-85729-327-5. doi: 10.1007/978-0-85729-327-5. URL <http://link.springer.com/10.1007/978-0-85729-327-5>.

- [5] Dong, R., Li, B., and Chen, Q.-m. An Automatic Calibration Method for PTZ Camera in Expressway Monitoring System. In *2009 WRI World Congress on Computer Science and Information Engineering*, volume 6, pp. 636–640, March 2009. doi: 10.1109/CSIE.2009.763.
- [6] Dubska, M., Herout, A., and Sochor, J. Automatic Camera Calibration for Traffic Understanding. In *Proceedings of the British Machine Vision Conference 2014*, pp. 42.1–42.12, Nottingham, 2014. British Machine Vision Association. ISBN 978-1-901725-52-0. doi: 10.5244/C.28.42. URL <http://www.bmva.org/bmvc/2014/papers/paper013/index.html>.
- [7] Faugeras, O. *Three-dimensional computer vision: a geometric viewpoint*. MIT Press, 1993.
- [8] Fung, G. S. K. Camera calibration from road lane markings. *Optical Engineering*, 42(10):2967, October 2003. ISSN 0091-3286. doi: 10.1117/1.1606458. URL <http://opticalengineering.spiedigitallibrary.org/article.aspx?doi=10.1117/1.1606458>.
- [9] HM Government. Open Government Licence, 2020. URL <http://www.nationalarchives.gov.uk/doc/open-government-licence/version/3/>.
- [10] Lai, A. H. S., Yung, N. H. C., and Member, S. Lane detection by orientation and length discrimination. *IEEE Trans. Syst., Man, Cybern. B*, pp. 539–548, 2000.
- [11] Liebowitz, D. and Zisserman, A. Metric rectification for perspective images of planes. In *Proceedings. 1998 IEEE Computer Society Conference on Computer Vision and Pattern Recognition (Cat. No.98CB36231)*, pp. 482–488, June 1998. doi: 10.1109/CVPR.1998.698649. ISSN: 1063-6919.
- [12] Lin, T.-Y., Maire, M., Belongie, S., Hays, J., Perona, P., Ramanan, D., Dollár, P., and Zitnick, C. L. Microsoft COCO: Common Objects in Context. In Fleet, D., Pajdla, T., Schiele, B., and Tuytelaars, T. (eds.), *Computer Vision – ECCV 2014*, Lecture Notes in Computer Science, pp. 740–755, Cham, 2014. Springer International Publishing. ISBN 978-3-319-10602-1. doi: 10.1007/978-3-319-10602-1\_48.
- [13] Liu, W., Anguelov, D., Erhan, D., Szegedy, C., Reed, S., Fu, C.-Y., and Berg, A. C. Ssd: Single shot multibox detector, 2015.
- [14] Luo, Z., Branchaud-Charron, F., Lemaire, C., Konrad, J., Li, S., Mishra, A., Achkar, A., Eichel, J., and Jodoin, P.-M. MIO-TCDD: A New Benchmark Dataset for Vehicle Classification and Localization. *IEEE Transactions on Image Processing*, 27(10):5129–5141, October 2018. ISSN 1941-0042. doi: 10.1109/TIP.2018.2848705. Conference Name: IEEE Transactions on Image Processing.
- [15] Matters, T. f. L. l. E. J. Our open data, 2020. URL <https://www.tfl.gov.uk/info-for/open-data-users/our-open-data>.
- [16] May, T. Lockdown-type measures look effective against covid-19. *BMJ*, 370, July 2020. ISSN 1756-1833. doi: 10.1136/bmj.m2809. URL <https://www.bmj.com/content/370/bmj.m2809>. Publisher: British Medical Journal Publishing Group Section: Editorial.
- [17] Redmon, J. and Farhadi, A. Yolov3: An incremental improvement, 2018.
- [18] Schoepflin, T. N. and Dailey, D. J. Dynamic camera calibration of roadside traffic management cameras for vehicle speed estimation. *IEEE Transactions on Intelligent Transportation Systems*, 4(2):90–98, 2003.
- [19] Schoepflin, T. N., Dailey, D. J., et al. Algorithms for estimating mean vehicle speed using uncalibrated traffic management cameras. Technical report, Washington (State). Dept. of Transportation, 2003.
- [20] Sekachev, B., Manovich, N., Zhiltsov, M., Zhavoronkov, A., Kalinin, D., Hoff, B., TOSmanov, Kruchinin, D., Zankevich, A., DmitriySidnev, Markelov, M., Johannes222, Chenuet, M., a andre, telenachos, Melnikov, A., Kim, J., Ilouz, L., Glazov, N., Priya4607, Tehrani, R., Jeong, S., Skubriev, V., Yonekura, S., vugia truong, zliang7, lizhming, and Truong, T. opencv/cvat: v1.1.0, August 2020. URL <https://doi.org/10.5281/zenodo.4009388>.

- [21] Shapiro, L. and Stockman, G. *Computer Vision*. Prentice House London, 2001.
- [22] Song, K.-T. and Tai, J.-C. Dynamic Calibration of Pan–Tilt–Zoom Cameras for Traffic Monitoring. *IEEE Transactions on Systems, Man and Cybernetics, Part B (Cybernetics)*, 36(5): 1091–1103, October 2006. ISSN 1083-4419. doi: 10.1109/TSMCB.2006.872271. URL <http://ieeexplore.ieee.org/document/1703651/>.
- [23] Tsai, R. A versatile camera calibration technique for high-accuracy 3d machine vision metrology using off-the-shelf tv cameras and lenses. *IEEE Journal on Robotics and Automation*, 3(4): 323–344, 1987.
- [24] Zhang, Z., Tan, T., Huang, K., and Wang, Y. Practical Camera Calibration From Moving Objects for Traffic Scene Surveillance. *IEEE Transactions on Circuits and Systems for Video Technology*, 23(3):518–533, March 2013. ISSN 1558-2205. doi: 10.1109/TCSVT.2012.2210670. Conference Name: IEEE Transactions on Circuits and Systems for Video Technology.

## Appendix A Deployment

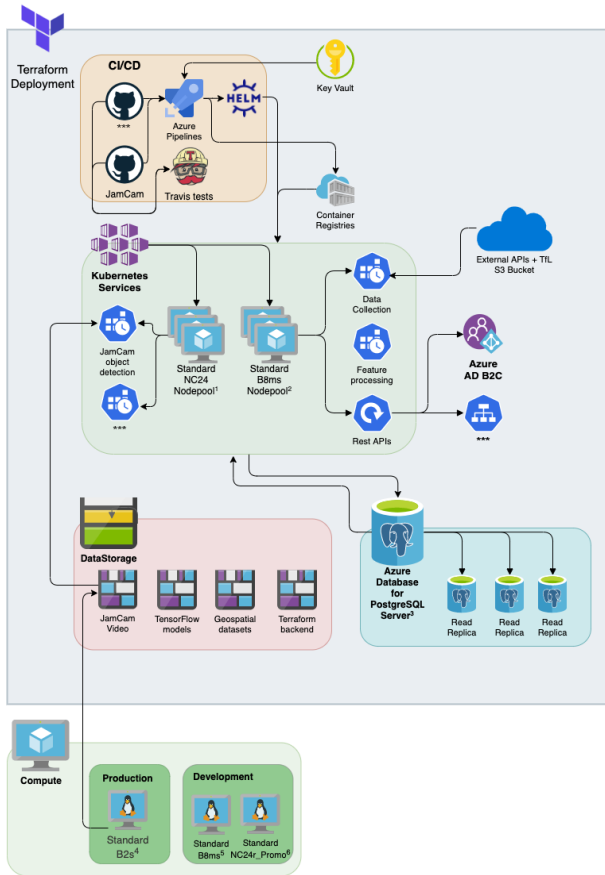


Figure A.1: Project architecture. Deployment provisioning is controlled declaratively by Terraform, containing each component of the processing pipeline. Kubernetes manages two compute clusters: (1) A GPU accelerated horizontally scaled video processing pool; (2) A stability focused horizontally scaled burstable CPU pool executing scheduled tasks and hosting API access points for direct data acquisition and service for control centre output, Figure A.2.

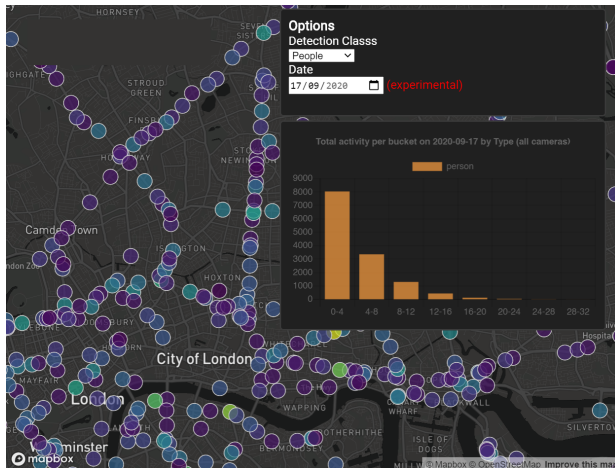


Figure A.2: Control centre output. Provides real-time interactive pan-London activity metrics in web application format convenient to stakeholders.



## Appendix B Intermediate Camera Planes

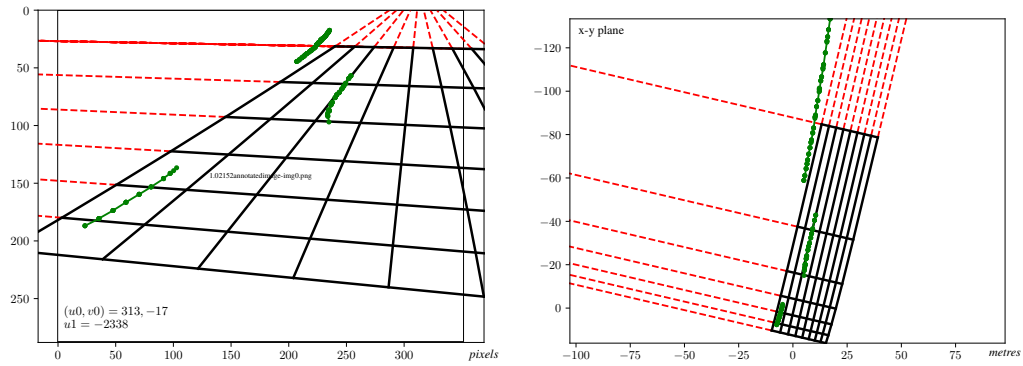


Figure B.1: Demonstration of perspective mapping of camera calibration from image to world plane before estimated registration to British National Grid. Rays (black, solid) are drawn as grid lines and extended (red, dashed) to the estimated vanishing points  $(u_0, v_0)$  and  $(u_1, v_0)$ . When mapped onto world coordinates. For example, vehicle trajectories (green, dotted) are mapped by this transformation.